

Frequency-Aware Model Predictive Control

Ruben Grandia¹, Farbod Farshidian¹, Alexey Dosovitskiy², René Ranftl², Marco Hutter¹

Abstract— Transferring solutions found by trajectory optimization to robotic hardware remains a challenging task. When the optimization fully exploits the provided model to perform dynamic tasks, the presence of unmodeled dynamics renders the motion infeasible on the real system. Model errors can be a result of model simplifications, but also naturally arise when deploying the robot in unstructured and nondeterministic environments. Predominantly, compliant contacts and actuator dynamics lead to bandwidth limitations. While classical control methods provide tools to synthesize controllers that are robust to a class of model errors, such a notion is missing in modern trajectory optimization, which is solved in the time domain. We propose frequency-shaped cost functions to achieve robust solutions in the context of optimal control for legged robots. Through simulation and hardware experiments we show that motion plans can be made compatible with bandwidth limits set by actuators and contact dynamics. The smoothness of the model predictive solutions can be continuously tuned without compromising the feasibility of the problem. Experiments with the quadrupedal robot ANYmal, which is driven by high-compliant series elastic actuators, showed significantly better tracking performance of the planned motion, torque, and force trajectories and enabled the machine to walk robustly on ground with unmodeled compliance.

I. INTRODUCTION

Trajectory optimization based on the full dynamics of a robotic system provides a flexible tool to generate complex motion plans for robots. It enables the system to exploit the full dynamic capabilities of the robot to achieve a task. State-of-the-art approaches are able to rapidly find solutions while incorporating increasingly complex model descriptions, which allows using trajectory optimization in a model predictive control (MPC) fashion. However, relying on the specific structure of the model makes implementation of the synthesized motion plans prone to modeling errors. Executing motion plans on hardware has therefore proven to be nontrivial and often requires manual, task-dependent tuning of cost functions and constraints to achieve feasible motions.

A major source of modeling error is the treatment of actuators as perfect torque sources. Any real system is subject to bandwidth limits and as such is not an ideal torque source. Current approaches for trajectory optimization neglect this effect and find motion plans that change torque

*This research was supported by Intel Network on Intelligent Systems, the Swiss National Science Foundation through the National Centre of Competence in Research Robotics (NCCR Robotics), the European Unions Horizon 2020 research and innovation programme under grant agreement No 780883. This work has been conducted as part of ANYmal Research, a community to advance legged robotics.

¹ First, second, and last author are with Robotic Systems Lab, ETH Zurich, Switzerland rgrandia@ethz.ch ² Third, and fourth author are with Intel Labs, Munich, Germany

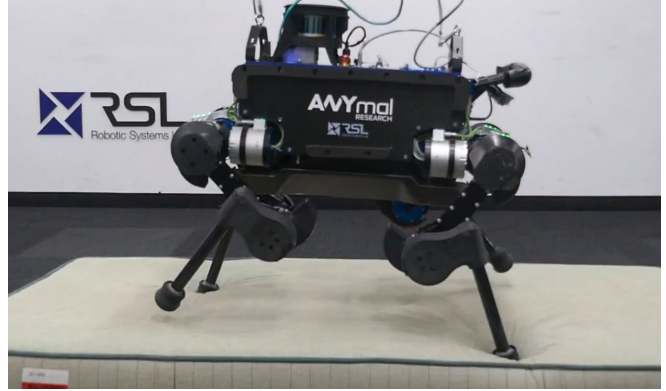


Fig. 1. The quadruped robot ANYmal [1] trotting in place on non-rigid terrain. This experimental setup is used to test the controller's robustness against unmodeled contact dynamics.

instantaneously, making it impossible to track the plans on the hardware. A similar modeling error occurs when assuming a rigid contact with the ground, which generally does not hold during locomotion in outdoor environments or on compliant surfaces as shown in Fig. 1. The rigid contact essentially provides the optimizer with infinite bandwidth on the contact forces. As a result, motion plans generated assuming idealized contact and actuator dynamics cannot be tracked by the hardware, leading to failure of the locomotion controller.

In this paper, we extend model predictive control (MPC) methods for legged robots to situations where the assumptions of rigid ground and perfect actuators are invalid. We address the issues of inherent bandwidth limits in real robots by adapting the cost function to be frequency-dependent, making it possible to penalize high frequencies in the motion plans. As a result, instantaneous changes to torque or ground reaction forces (GRF) are avoided. The solver, therefore, does not have to reason about the exact details of terrain and actuator dynamics but will produce solutions that are achievable under the bandwidth limits. We show that motion plans generated with our frequency-aware trajectory optimization can be followed by the hardware more accurately than those generated with a standard baseline and enables locomotion on compliant terrain.

A. Related work

To increase the feasibility of optimized motions several aspects of the problem can be modified. In general, one can classify such efforts in adaptations of the cost function, model, or constraints. Independent of the strategy, one typically needs to strike a balance between ensuring compatibility

ity with hardware and restricting the solution space.

In case of a series elastic actuator, the dynamics can be approximated and added to the model. The optimization algorithm is in those cases able to exploit the properties of the specific actuator and adding spring-damper elements to the joints is even known to result in motions that resemble those found in nature [2]. For series elastic actuators, methods have been proposed to incorporate bandwidth, torque, and joint limits in a computationally efficient way [3][4][5]. However, very often we don't have exact details of actuators and modeling them would lead to high engineering effort. Moreover, since parts of the underlying actuator dynamics have very different time constants, smaller timesteps leading to slower update rates prevent such models from use in MPC with complex systems. Additionally, stability problems can arise when a limb with stiffly modeled actuators makes contact with the environment [6]. We avoid such issues by not explicitly modelling the actuators, but by incorporating well-known bandwidth limitations up to which the perfect tracking assumption is valid.

While model parameters for actuators can be obtained from first principles or through repeated experiments, contact dynamics are considerably harder to model or predict. A combination of learning a terrain model and trajectory optimization has been proposed in [7]. However, such methods have not reached real-time capabilities, and the question of how to optimize without prior knowledge of an unknown terrain remains unanswered.

In the context of contact invariant optimization, soft contact models [8] or contact smoothing [9] are used inside trajectory optimization. These models are selected and tuned for their numerical properties rather than physical accuracy. The models need to be smooth since the highly coupled interaction between stiff contact dynamics and slow dynamics of the robot lead to poor convergence of the algorithms. In the worst case, this numeric model tuning can lead to highly undesired effects when the optimizer starts exploiting dynamic properties of the terrain which are entirely wrong.

Instead of adapting the model, a smooth parameterization of the trajectories can be imposed to ensure feasibility. This common technique is found in spline based optimization [10], [11], collocation methods [12], [13], or when using dynamic motion primitives [14]. This, however, limits the motions that can be expressed and can often require a problem specific, manual tuning procedure.

As an alternative to adapting the model or constraints, we propose to encode bandwidth limits through the cost function. A trivial way to do so is to put extra costs on input signals, but this results in slower response overall and goes against the desire to perform highly dynamic motions at the limits of the system. Instead, we intend to explore a slightly different approach and propose to use a frequency-dependent cost function [15]. We penalize control actions only in the high frequency range and combine this idea with a modern optimal control framework [16], [17].

Perhaps the closest related idea in recent literature is found in [18], where a constraint is formed in the frequency

domain. Since the locomotion problem already has numerous constraints, we prefer to use the cost function approach instead of adding more hard constraints that increase the risk of an infeasible solution. Additionally, the proposed window based constraints approach requires previous and future decision variables, which negatively affects the Riccati-sparsity pattern exploited in optimal control methods.

B. Contributions

We introduce frequency-dependent cost functions integrated into modern MPC strategies for legged locomotion. Through simulation experiments, we study the effect of such a cost function on the resulting solutions. The proposed method provides the user with an intuitive way to achieve robustness against unmodeled phenomena like actuator bandwidth limits and non-rigid contact dynamics. These findings were successfully validated in hardware experiments on different grounds. Using frequency-shaped cost functions, we could improve the robustness of ANYmal while locomoting under substantial external disturbances coming from external pushed or unmodeled soft ground.

II. METHOD

First, we discuss uncertainty in the dynamics from a robustness point of view and motivate the particular choice of cost functions. Afterward, the integration with a sequential linear quadratic model predictive control (SLQ-MPC) method [17] is presented. This method, based on Differential Dynamic Programming (DDP), relies on a linear approximation of the dynamics and a quadratic approximation of the cost function around the latest trajectory.

For brevity of notation in the current section, and without loss of generality, we consider the following quadratic cost function without linear and mixed state-input costs,

$$J = \frac{1}{2} \int_0^\infty \mathbf{x}(t)^T \mathbf{Q} \mathbf{x}(t) + \mathbf{u}(t)^T \mathbf{R} \mathbf{u}(t) dt, \quad (1)$$

where \mathbf{Q} is the positive semi-definite state cost Hessian and \mathbf{R} is the positive definite input cost Hessian.

A. High frequency robustness

Consider a linear plant $G(j\omega)$ with unstructured multiplicative uncertainty model $L(j\omega)$,

$$G'(j\omega) = [I + L(j\omega)]G(j\omega), \quad (2)$$

with

$$\bar{\sigma}[L(j\omega)] < l_m(\omega), \quad \forall \omega \geq 0, \quad (3)$$

where $\bar{\sigma}$ is the maximum singular value of the disturbance model and $l_m(\omega)$ is a frequency-dependent upper bound. The closed loop stability condition for these models is [19],

$$l_m(\omega) < \sigma[I + GK(j\omega)^{-1}], \quad (4)$$

where σ is the minimum singular value, and $GK(j\omega)$ is the transfer function of plant and controller together.

To be robust against large uncertainties at high frequencies, according to (4), the loop gain, $GK(j\omega)$, should be

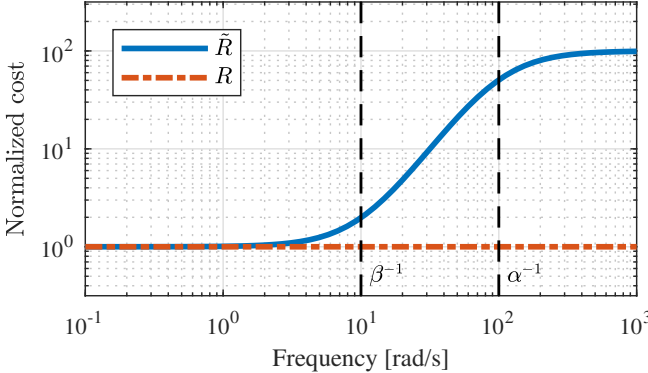


Fig. 2. Example of the frequency-shaped cost function for $\alpha = 0.01$, $\beta = 0.1$, and the standard input costs in the frequency domain. Costs are normalized by R .

kept low. Intuitively, penalizing inputs at the high frequencies reduces the feedback gain at those frequencies, which allows for larger uncertainty magnitude, $l_m(\omega)$. We therefore propose to use the following frequency-dependent input weighting

$$\tilde{R}(\omega) = \left| \frac{1 + \beta j\omega}{1 + \alpha j\omega} \right|^2 R, \quad \text{with } \beta > \alpha \quad (5)$$

where R is the original input cost, and $-\beta^{-1}$ and $-\alpha^{-1}$ are the zero and pole of the loopshaping transfer function. A visualization of such cost function is provided in Fig. 2. This cost function is of similar shape as the disturbance model proposed in [20], which highlights the close relation between disturbance modelling and cost function shaping.

Indeed, for Single-Input-Single-Output (SISO) systems Anderson *et al.* [21] established that the open loop gain at high frequency under the frequency-shaped cost function (5) is reduced, i.e. $|GK_{\tilde{R}}(j\omega)| < |GK_R(j\omega)|$. According to (4), the resulting increase in $\sigma[I + GK(j\omega)^{-1}]$ permits a higher model uncertainty in the stopband. At the same time, some gain and phase margins in the passband are lost, with associated decrease in robustness in the passband.

Moreover, the condition on α for the resulting controller to contain lag compensation is that *the open-loop plant has zero, or an even number of, positive real poles greater than α^{-1}* [22]. The transfer function pole, α^{-1} , in Fig. 2 thus has to exceed the fastest unstable pole of the system.

Unfortunately, to the best of our knowledge, a robustness proof for MIMO systems is not available. Despite that, the intuition that penalizing high frequency input increases compatibility with actuator bandwidth limits remains. In this paper, we aim to empirically validate the effect of using such a cost function.

B. frequency-shaped cost functions

MPC plans over a receding horizon. The cost function in (5) therefore needs to be expressed in the time domain as well. This can be achieved by a state augmentation as described in [15]. We repeat the essential steps for completeness.

The standard quadratic cost function for the time domain (1) can be converted to the frequency domain (6) according to Parseval's theorem:

$$J = \frac{1}{2\pi} \int_{-\infty}^{\infty} \mathbf{x}(\omega)^H \mathbf{Q} \mathbf{x}(\omega) + \mathbf{u}(\omega)^H \mathbf{R} \mathbf{u}(\omega) d\omega, \quad (6)$$

where $(\cdot)^H$ is the Hermitian transpose of the vector. Here, it becomes apparent that the standard costs over states and inputs are constant for all frequencies. To leave the possibility of having different loopshaping per input dimension, the frequency-dependent weight matrix in (5) is generalized to

$$\tilde{\mathbf{R}}(\omega) = \begin{bmatrix} r_1^*(\omega) & & & \\ & \ddots & & \\ & & r_m^*(\omega) & \end{bmatrix} \mathbf{R} \begin{bmatrix} r_1(\omega) & & & \\ & \ddots & & \\ & & r_m(\omega) & \end{bmatrix}$$

with

$$r_i(\omega) = \frac{1 + \beta_i j\omega}{1 + \alpha_i j\omega}, \quad (7)$$

where $r_i^*(\omega)$ is the complex conjugate of $r_i(\omega)$. Every input directions can now have its own shaping function r_i . In order to transfer this new cost function back into the time domain, a change of variables is required. The filtered inputs, $\mathbf{v}(\omega)$, are defined as

$$v_i(\omega) = r_i(\omega) u_i(\omega). \quad (8)$$

After substitution, we arrive back at a frequency independent cost function over the filtered variables in (10). This cost is then converted back to the time domain in (11),

$$J = \frac{1}{2\pi} \int_{-\infty}^{\infty} \mathbf{x}(\omega)^H \mathbf{Q} \mathbf{x}(\omega) + \mathbf{u}(\omega)^H \tilde{\mathbf{R}}(\omega) \mathbf{u}(\omega) d\omega \quad (9)$$

$$= \frac{1}{2\pi} \int_{-\infty}^{\infty} \mathbf{x}(\omega)^H \mathbf{Q} \mathbf{x}(\omega) + \mathbf{v}(\omega)^H \mathbf{R} \mathbf{v}(\omega) d\omega \quad (10)$$

$$= \frac{1}{2} \int_0^{\infty} \mathbf{x}(t)^T \mathbf{Q} \mathbf{x}(t) + \mathbf{v}(t)^T \mathbf{R} \mathbf{v}(t) dt \quad (11)$$

In this work, we keep the original inputs as decision variables and thus require slight costs on $\mathbf{u}(t)$ to obtain a positive definite cost matrix. We therefore interpolate between (6) and (11) and obtain

$$J = \frac{1}{2} \int_0^{\infty} \mathbf{x}(t)^T \mathbf{Q} \mathbf{x}(t) + \gamma \mathbf{v}(t)^T \mathbf{R} \mathbf{v}(t) + (1 - \gamma) \mathbf{u}(t)^T \mathbf{R} \mathbf{u}(t) dt. \quad (12)$$

To compute the filtered inputs $\mathbf{v}(t)$, the state space realization of the transfer functions $r_i^{-1}(\omega)$ is used,

$$\dot{x}_{f,i} = A_{f,i} x_{f,i} + B_{f,i} v_i, \quad (13)$$

$$u_i = C_{f,i} x_{f,i} + D_{f,i} v_i. \quad (14)$$

The system dynamics $\dot{\mathbf{x}} = \mathbf{f}(\mathbf{x}, \mathbf{u})$ should then be extended to

$$\begin{bmatrix} \dot{\mathbf{x}} \\ \dot{\mathbf{x}}_f \end{bmatrix} = \begin{bmatrix} \mathbf{f}(\mathbf{x}, \mathbf{u}) \\ \mathbf{A}_f \mathbf{x}_f + \mathbf{B}_f \mathbf{v} \end{bmatrix}, \quad (15)$$

with constraints

$$\begin{bmatrix} g(\mathbf{x}, \mathbf{u}) \\ \mathbf{C}_f \mathbf{x}_f + \mathbf{D}_f \mathbf{v} - \mathbf{u} \end{bmatrix} = \mathbf{0}, \quad (16)$$

and cost matrices adapted as

$$\hat{\mathbf{Q}} = \begin{bmatrix} \mathbf{Q} & \mathbf{0} \\ \mathbf{0} & \mathbf{0} \end{bmatrix}, \quad \hat{\mathbf{R}} = \begin{bmatrix} (1-\gamma)\mathbf{R} & \mathbf{0} \\ \mathbf{0} & \gamma\mathbf{R} \end{bmatrix}. \quad (17)$$

Throughout this work, we use $\gamma = 0.9$. Ideally, one would let γ approach 1.0 to reach the pure frequency-dependent cost function in (12), but this results in a bad condition number of $\hat{\mathbf{R}}$ in (17). The current value was therefore selected as a compromise for numerical reasons.

C. Variations

Note that it is also possible to use the state space realization of $r_i(\omega)$, without the inversion. This, however, results in faster filter dynamics because \mathbf{A}_f would correspond to the fast pole $-\alpha^{-1}$ instead of the slower pole of the inverse, $-\beta^{-1}$. We prefer the slower filter dynamics to allow the continuous time forward integration in the SLQ-MPC to use larger time-steps.

Moreover, (14) can be substituted into $\mathbf{f}(\mathbf{x}, \mathbf{u})$ and $\mathbf{g}(\mathbf{x}, \mathbf{u})$ directly instead of adding it as a constraint. However, keeping both decision variables gives the solver more degrees of freedom in intermediate steps and leaves the original system dynamics and constraints untouched. Since we want to interfere with the nominal problem as little as possible, we opt for the latter. Such a strategy, known as *lifting* [23], is a commonly used method to increase the region of convergence and contraction rates of Newton type algorithms.

A detailed study of the numerical properties of each equivalent reformulation is beyond the scope of this paper. We are rather interested in the effect that the cost function shaping has on the solutions of the optimal control problem.

The option to constrain the input rate can also be interpreted as a frequency-dependent weighting, where the weight is given by $r(\omega) = j\omega$. Implementing this in an MPC framework requires one to use the original input as a state and have the input rate as the new inputs. This turns state-input constraints into pure state constraints, which are more computationally expensive to handle. Retaining the original input alongside the input rate analogous to (16) does not remedy this since $D_f = 0$ for filters that are not of relative degree 0, which leads to an overconstrained problem.

III. EXPERIMENTAL SETUP

A. Problem Formulation

The proposed method is applied to the kinodynamic model of a quadruped robot, which describes the dynamics of a single free-floating body along with the kinematics for each leg [17]. The Equations of Motion (EoM) are given by

$$\begin{cases} \dot{\boldsymbol{\theta}} = \mathbf{T}(\boldsymbol{\theta})\boldsymbol{\omega} \\ \dot{\mathbf{p}} = {}_W\mathbf{R}_B(\boldsymbol{\theta})\mathbf{v} \\ \dot{\boldsymbol{\omega}} = \mathbf{I}^{-1} \left(-\boldsymbol{\omega} \times \mathbf{I}\boldsymbol{\omega} + \sum_{i=1}^4 \mathbf{r}_{EEi}(\mathbf{q}) \times \boldsymbol{\lambda}_{EEi} \right) \\ \dot{\mathbf{v}} = \mathbf{g}(\boldsymbol{\theta}) + \frac{1}{m} \sum_{i=1}^4 \boldsymbol{\lambda}_{EEi} \\ \dot{\mathbf{q}} = \mathbf{u}_J, \end{cases}$$

where ${}_W\mathbf{R}_B$ and \mathbf{T} are the rotation matrix of the base with respect the global frame and the transformation matrix from angular velocities in the base frame to the Euler angles derivatives in the global frame. \mathbf{g} is the gravitational acceleration in body frame, \mathbf{I} and m are the moment of inertia about the CoM and the total mass respectively. The inertia is assumed to be constant and taken at the default configuration of the robot. \mathbf{r}_{EEi} is the position of the foot i with respect to CoM. $\boldsymbol{\theta}$ is the orientation of the base in Euler angles, \mathbf{p} is the position of the CoM in world frame, $\boldsymbol{\omega}$ is the angular rate, and \mathbf{v} is the linear velocity of the CoM. The inputs of the model are the joint velocity commands \mathbf{u}_J and end effector contact forces $\boldsymbol{\lambda}_{EEi}$.

The constraints depending on the mode of a leg at that point in time are formulated as

$$\begin{cases} \mathbf{u}_{EEi} = \mathbf{0} & \text{if } i \text{ is a stance leg} \\ \mathbf{u}_{EEi} \cdot \hat{\mathbf{n}} = c(t), \quad \boldsymbol{\lambda}_{EEi} = \mathbf{0}, & \text{if } i \text{ is a swing leg} \end{cases}$$

where \mathbf{u}_{EEi} is the end effector velocity in world frame, which constrains a stance leg to remain on the ground and a swing leg to follow the predefined curve $c(t)$ normal to the surface in order to avoid foot scoffing with zero contact force inputs $\boldsymbol{\lambda}_{EEi}$.

The baseline cost is formulated as a quadratic function

$$J = \frac{1}{2} \int_0^T (\mathbf{x}(t) - \mathbf{x}_d)^T \mathbf{Q} (\mathbf{x}(t) - \mathbf{x}_d) + (\mathbf{u}(t) - \mathbf{u}_0)^T \mathbf{R} (\mathbf{u}(t) - \mathbf{u}_0) dt, \quad (18)$$

where \mathbf{x}_d is a desired state consisting of commanded base pose and twist by the user and a default configuration for the joints. We use a simple diagonal cost on all state variables and contact force inputs. The joint velocities costs are a diagonal matrix pre and post multiplied by the end-effector Jacobians to weigh the costs in task space.

B. System integration

In the model described in the previous section, the control inputs are end-effector forces and joint velocities. To translate the solution to torque commands, we extract a full position, velocity, and acceleration plan for CoM and end-effector trajectories, in addition to the planned contact forces. This plan is tracked by the hierarchical whole-body control (WBC) architecture described in [24]. The tasks in decreasing priority are (1) satisfying the equation of motions and zero acceleration for contact feet (2) tracking CoM and swing leg trajectories, and (3) tracking the planned contact forces. The desired contact forces from the MPC are thus communicated in two ways: The CoM trajectory dictates the net acting forces, and force tracking task regulates the internal forces. Without the latter, contact forces would be redistributed among the contacts, which would override the planned smoothness of the trajectories. Additionally, on all priorities, torque limits and friction cone constraints are imposed as inequality constraints.

The optimal control problem in (18) is solved for a user-defined gait with the continuous time SLQ-MPC algorithm described in [16]. We use a receding horizon length of 1.0s,

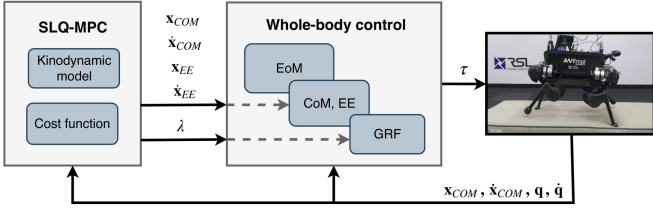


Fig. 3. MPC and whole-body control structure overview. The SLQ-MPC algorithm running on a separate desktop PC sends center of mass (CoM) and end-effector (EE) reference to the onboard whole-body control structure. This hierarchical controller with priorities listed from high to computes torque commands.

which results in an MPC update rate of 70Hz for the baseline method and around 40Hz for the frequency-shaped method.

The MPC runs on a desktop PC with an Intel Core i7-8700K CPU@3.70GHz hexacore processor and continuously computes a motion plan from the latest known state through a real-time-iteration scheme. The WBC runs on the dedicated onboard PC and tracks the most recent plan. Here, the augmented filter state is propagated as well according to (13) with the currently available augmented input plan $v(t)$. Both nodes communicate over a local ROS network. An overview of the experimental setup is provided in Fig. 3.

IV. RESULTS

We study the effects of adopting the cost function in (12) for the previously described setup under various locomotion tasks. To see the results at different levels of model errors, we conduct perfect model simulations, rigid-body simulations, and hardware experiments. When selecting different values for β , α is selected such that the frequencies in the stopband incur a cost of 100 times the DC cost, i.e. $\alpha = 0.1\beta$.

A. Perfect model

First, we investigate the effect of the loopshaping on the contact forces in a simulation that uses the same model as the MPC. This shows how the resulting trajectories are different already in the case of no modeling errors. The analyzed gait is a trot with a duty factor of 0.5, i.e. with no overlap in stance phases of the diagonal feet, while a forward velocity of 0.5 m/s is commanded. Figure 4 shows the ground reaction forces when selecting different values for β . As seen from the plot, the baseline method instantaneously applies contact forces once a foot is in contact. As expected, lowering the frequency at which costs start to increase, i.e. lowering β^{-1} , results in increasingly smooth trajectories. The frequency-shaped method approaches the baseline as β^{-1} goes to infinity. The corresponding base height trajectories are plotted in Fig. 5. Smoother contact force trajectories require more vertical displacement of the base, while the baseline produces the exact amount of force to keep the base level.

A similar experiment is conducted to see how frequency-shaped solutions behave for different gait periods. The period T of the trotting gait is varied for a fixed cost function with $\beta^{-1} = 25$. The resulting ground reaction forces are shown

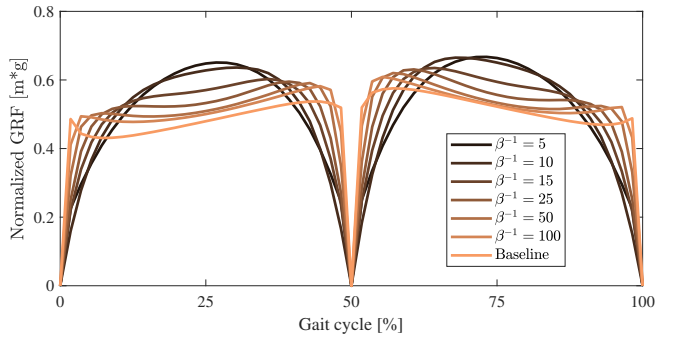


Fig. 4. Ground reaction forces in z-direction for a trotting gait at 0.5 m/s with a period of $T = 0.7$ s. The first half of the gait cycle corresponds to the left front foot and the second half to the left hind foot. As the frequency limit decreases from infinity (i.e., baseline) to 5, the smoothness of the planned contact forces increases.

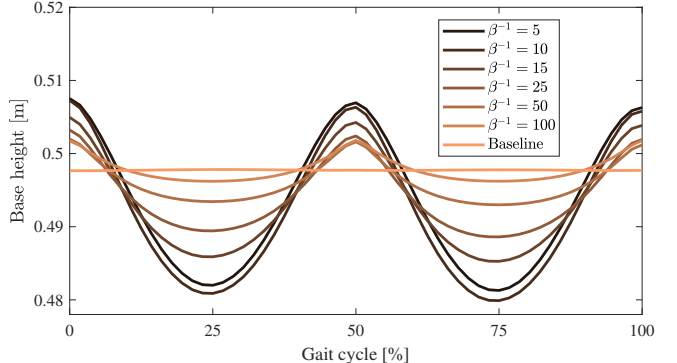


Fig. 5. Base height for a trotting gait at 0.5 m/s with a period of $T = 0.7$ s under different smoothing parameters. In general, the vertical displacement of the base increases as the controller becomes smoother since it cannot abruptly increase or decrease the ground reaction forces at the stance feet.

in Fig. 6. For the fixed smoothing parameter, the contact profile transitions from a two hump solution to a single hump solution as the gait period decreases. Interestingly, a similar pattern is observed for humans and quadrupeds [25].

B. Physics simulation

The combination of tracking controller and MPC is evaluated in the Open Dynamics Engine [26] rigid-body simulation, where we can vary ground properties in a controlled way. The model errors, in this case, come from the difference between rigid-body dynamics and the kinodynamic model, as well as the assumption of a rigid ground contact when the terrain is made compliant. ODE allows for simulation of soft contacts by modelling¹ the ground contact forces as a spring-damper system. Three different sets of spring-damper parameters k_p and k_d are selected to simulate hard, intermediate, and soft ground, respectively. For each terrain, three different cost functions are evaluated: the baseline without frequency shaping as well as frequency-dependent cost functions with $\beta^{-1} = 50$ and $\beta^{-1} = 10$. These values were selected based on Fig. 4 to represent three levels of smoothness in the continuum of available cost functions.

¹ODE relaxes the rigid-contact solver such that it implicitly resembles a spring-damper interaction.

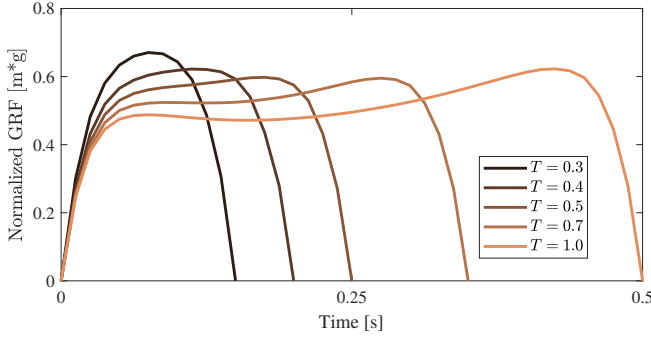


Fig. 6. Ground reaction forces during a trotting gait at 0.5 m/s for various periods T , with $\beta^{-1} = 25$. The first half of the gait cycle corresponding to the left front foot is plotted. As the gait period increases, a two hump solution transients to a single hump solution.

TABLE I

FORCE TRACKING PERFORMANCE MAE (MSE) [N (N²)] FOR DIFFERENT TERRAIN AND COST FUNCTION COMBINATIONS IN SIMULATION.

Terrain $\{k_p, k_d\}$	Cost function		
	Baseline	$\beta^{-1} = 50$	$\beta^{-1} = 10$
Hard $\{1e6, 100\}$	6.1 (751.9)	4.1 (256.9)	4.2 (230.2)
Medium $\{1e5, 50\}$	7.0 (353.4)	4.7 (114.3)	5.3 (130.8)
Soft $\{1e4, 30\}$	17.7 (742.0)	17.4 (543.9)	11.9 (251.7)

The resulting contact force profiles for all combinations are shown for a single stance phase in Fig. 7. Desired and measured contact forces are shown for a single leg during an in-place trotting motion with a stance duration of $T = 0.25$ s.

As the compliance of the terrain increases, the difference between desired forces generated from the WBC and resulting forces grows. The WBC uses rigid-body dynamics with a hard contact assumption to compute desired contact forces. The difference between desired and measured forces is therefore a measure of disturbances inserted by additional unmodeled dynamics, which in general includes the bandwidth limits of actuators and contact dynamics that we aim to avoid. Table I shows the force tracking performance averaged over six gait cycles in Mean Absolute Error (MAE) and Mean Squared Error (MSE) defined as

$$\text{MAE} = \frac{1}{T} \int_0^T |\boldsymbol{\lambda} - \boldsymbol{\lambda}_{des}| dt, \quad (19)$$

$$\text{MSE} = \frac{1}{T} \int_0^T (\boldsymbol{\lambda} - \boldsymbol{\lambda}_{des})^2 dt. \quad (20)$$

For all cost functions, tracking performance degrades as the model error increases. Qualitatively, the baseline controller suffers from a larger error at the beginning and end of the contact phase, due to its step-like change in the desired forces. Even on hard terrain, there is an apparent benefit of loopshaping. The smoother transition between contact phases mitigates the disturbance generated by contact timing mismatch. Differences become most apparent for the soft terrain, where the smoother trajectory has better performance in especially in MSE.

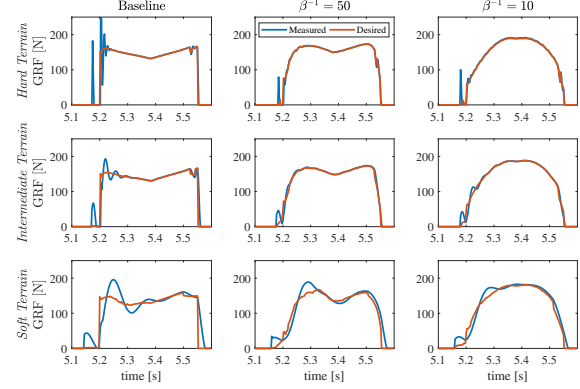


Fig. 7. Measured and desired contact forces in z-direction during a trot in-place for various ground properties and cost functions. The columns from left to right correspond to the baseline, $\beta^{-1} = 50$, and $\beta^{-1} = 10$ cost functions. The rows, from top to bottom corresponds to ground properties with k_p and k_d of $\{1e6, 100\}$, $\{1e5, 50\}$, and $\{1e4, 30\}$. As the compliance of the terrain increases, the difference between desired forces generated from the whole-body controller and resulting forces grows.

Furthermore, we examine the locomotion strategy under two extrema of cost functions. The commanded forward velocity during a trotting motion is gradually increased until failure occurs. The foot placement strategies are visualized in Fig. 8. The plots show footstep locations from a top-view with the robot starting at the origin. As the velocity increases towards the right side of the plot, the footstep locations start to differ. Interestingly, with the smoother cost function of $\beta^{-1} = 10$, the foot placement strategy is significantly altered and becomes velocity depend. Where under the baseline costs the controller chooses a fixed width foot placement, the frequency-shaped solution places the feet increasingly inwards for higher velocities. Remarkably, this results in a significantly higher maximum velocity of 0.77 m/s versus 0.52 m/s.

C. Hardware

On hardware, we aim to validate the simulation results for contact force tracking performance on different terrains. The floor of the lab, a 3.5 cm foam block, and a mattress are selected to test a rigid, an intermediate and a very compliant terrain. A force-torque sensor is mounted on the right front leg to obtain direct measurements of the ground reaction forces. The resulting measured and desired forces for different cost function and terrain combinations are shown in Fig. 9. The plots show the difference between measured and desired contact forces of the right-front leg during the first three steps. The MAE and MSE averaged over those first three gait cycles are given in Table II. On hard terrain, all methods perform well, and slight differences in tracking performance occur at the beginning and end of the contact phase. In this area the $\beta^{-1} = 10$ controller provides the smoothest transition, resulting in the best MAE and MSE on all terrains. That controller, however, has in return less accurate tracking during the middle of the stance phase. Where in the simulation experiments we see that a medium amount of smoothing is best for hard and medium

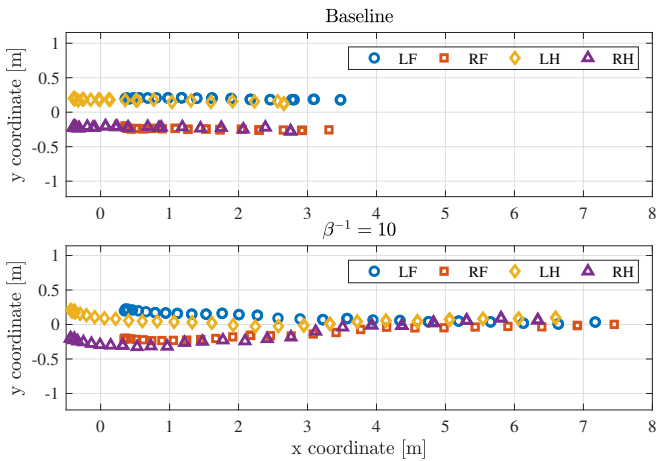


Fig. 8. Foot placement strategy for the baseline (top) and the $\beta^{-1} = 10$ (bottom) cost functions during a trot with increasing velocity commands in the positive x-direction. Commands start at $v = 0$ m/s and accelerate with 0.5 m/s 2 . Failure occurs at 0.52 m/s and 0.77 m/s respectively. The footstep strategy of the baseline method is different from the frequency-aware solution. While the former minimizes the lateral motion of the center of pressure by aligning the support polygons (lines), the baseline method does not adapt its footstep planning based on the velocity.

TABLE II
FORCE TRACKING PERFORMANCE MAE (MSE) [N (N 2)] FOR
DIFFERENT TERRAIN AND COST FUNCTION COMBINATIONS ON
HARDWARE.

Terrain	Cost function		
	Baseline	$\beta^{-1} = 50$	$\beta^{-1} = 10$
Hard	25.1 (2597.4)	21.2 (1696.8)	20.3 (1303.3)
Medium	22.1 (2044.6)	19.5 (1387.3)	18.5 (998.0)
Soft	37.9 (3470.6)	30.7 (2017.2)	22.1 (1022.4)

stiff terrain, we do not see this in the hardware experiments. The difference comes from the fact that ANYmal has series elastic actuators, causing model errors and bandwidth limits even on hard terrain. For a step input to the torque level reached during trot, a 90% rise-time up to 35 ms, equivalent to a bandwidth of around 60 rad/s can be expected [1].

When further reducing the compliance by trotting on the mattress, the baseline and $\beta^{-1} = 50$ controllers suffer a substantial decrease in performance. The base height during the first part of the experiment is shown in Fig. 10. Due to the significant mismatch between the planned and resulting contact force with each footstep, the baseline controller loses base height in a few steps, causing it to fail. The $\beta^{-1} = 50$ cost function does achieve a trot, as shown in the video², but strong oscillations are present between the terrain and the feet. The $\beta^{-1} = 10$ cost function, finally, results in both a stable trot and a smooth contact interaction.

In the accompanying video, we additionally show the behavior under disturbances. The robot trots in place and has costs on base deviation from the initial position. We disturb the robot in the horizontal plane. Qualitatively, the reactive stepping and push-back behavior differ. Under the

baseline method, the robot reacts to a push by generating lateral forces and the user experiences instant resistance. The frequency-aware implementation with $\beta^{-1} = 10$ instead accepts deviation of the base trajectory and adapts future step location and force profile to smoothly return to the origin.

V. DISCUSSION

We have shown that a single parameter of a frequency-dependent cost function provides a handle on a rich variety of solutions. While the smoothness at the beginning of the stance phase is not surprising due to the filter, the anticipatory decrease in force before lifting the foot, as seen in Fig. 4, shows that the filter and planning are tightly working together. The additional filter states allow the Riccati-type algorithm to reason about future state-input constraints, in this case, zero contact forces during the swing, and adapts the strategy to approach them smoothly. This is remarkable because the backward pass is projected on those constraints only at the point in time that they are active. Interestingly we also find that the foot placement strategy changes significantly. These observations highlight the fact that embedding frequency awareness of the MPC is richer than simply filtering the obtained inputs. As a future work, we will explore ways to change to cost function online and in this way adapt the locomotion strategy to the terrain.

A further opportunity arises when the gait is part of the motion optimization. As shown in Fig. 6, there is an interplay between the gait and the obtained contact force profiles. frequency-dependent costs could therefore be used to drive gait selection through optimization.

VI. CONCLUSION

We introduced frequency-aware MPC by combining frequency-dependent cost functions with modern MPC methods. With simulation experiments, we show that the resulting smoother force profiles improve tracking performance when the rigid terrain assumption is relaxed, without the need to explicitly model it. We validated these results on hardware and see a similar trend when comparing performance on various terrains. The method is shown to provide robustness against unmodeled dynamics of series elastic actuators and compliant terrains. We demonstrated that with this approach ANYmal is now able to execute dynamic motions even on highly compliant terrains.

REFERENCES

- [1] M. Hutter, C. Gehring, D. Jud, A. Lauber, C. D. Bellicoso, V. Tsounis, J. Hwangbo, K. Bodie, P. Fankhauser, M. Bloesch, *et al.*, “ANYmal - a highly mobile and dynamic quadrupedal robot,” in *IROS*, 2016, pp. 38–44.
- [2] G. Schultz and K. Mombaur, “Modeling and optimal control of human-like running,” *IEEE/ASME Transactions on Mechatronics*, vol. 15, no. 5, pp. 783–792, Oct 2010.
- [3] J. Nakanishi and S. Vijayakumar, “Exploiting passive dynamics with variable stiffness actuation in robot brachiation,” in *Proceedings of Robotics: Science and Systems*, Sydney, Australia, July 2012.
- [4] D. J. Braun, F. Petit, F. Huber, S. Haddadin, P. van der Smagt, A. Albu-Schaffer, and S. Vijayakumar, “Robots driven by compliant actuators: Optimal control under actuation constraints,” *IEEE Transactions on Robotics*, vol. 29, no. 5, pp. 1085–1101, Oct 2013.

²https://youtu.be/Mk_AjNnp6t0

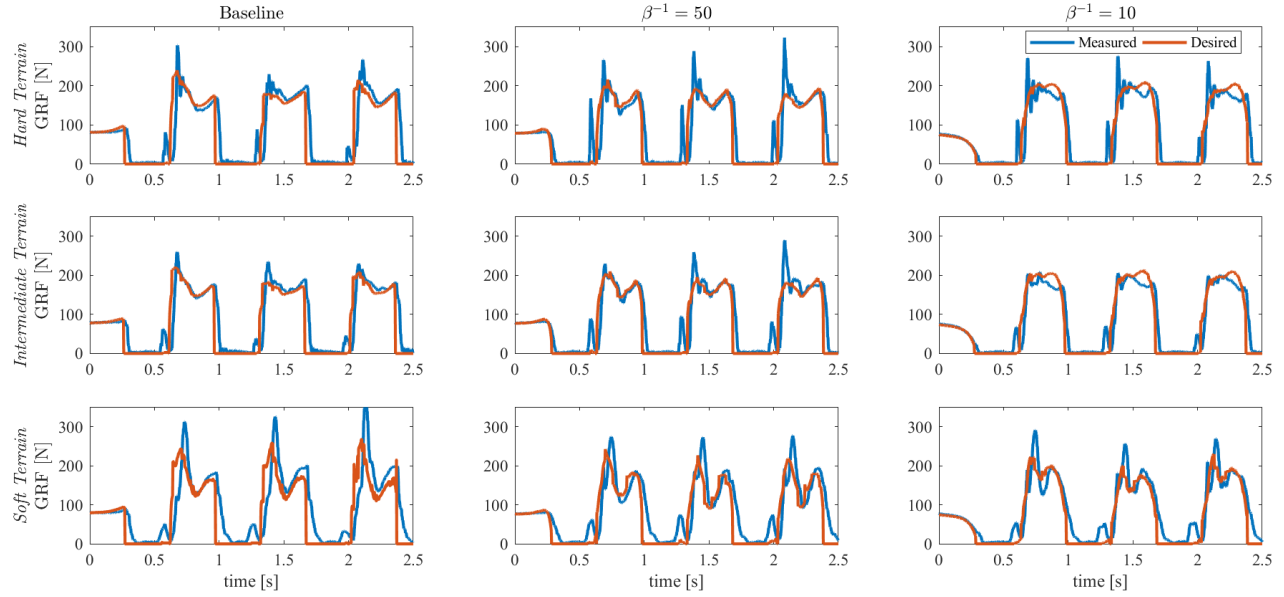


Fig. 9. Measured and desired contact forces for the right front foot during the first three trotting gait cycles on the lab floor (top row), foam (middle row) and a mattress (bottom row) with the baseline (left column), $\beta^{-1} = 50$ (middle column), and $\beta^{-1} = 10$ (right column) cost functions. A smoother transition between swing and stance phase results in better tracking performance.

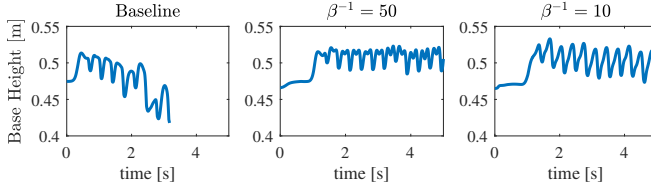


Fig. 10. Measured base height during the first 5 seconds of trotting motion on the mattress with the baseline (left column), $\beta^{-1} = 50$ (middle column), and $\beta^{-1} = 10$ (right column) cost functions. Where the baseline method fails to maintain its height, the frequency-aware controller remain stable.

- [5] R. Schlossman, G. C. Thomas, and L. Sentis, “Exploiting the natural dynamics of series elastic robots by actuator-centered sequential linear programming,” *arXiv preprint arXiv:1802.10190*, 2018.
- [6] J. Koenemann, A. D. Prete, Y. Tassa, E. Todorov, O. Stasse, M. Bennewitz, and N. Mansard, “Whole-body model-predictive control applied to the hrp-2 humanoid,” in *IROS*, 2015, pp. 3346–3351.
- [7] A. H. Chang, C. M. Hubicki, J. J. Aguilar, D. I. Goldman, A. D. Ames, and P. A. Vela, “Learning to jump in granular media: Unifying optimal control synthesis with gaussian process-based regression,” in *ICRA*, May 2017, pp. 2154–2160.
- [8] M. Neunert, F. Farshidian, A. W. Winkler, and J. Buchli, “Trajectory optimization through contacts and automatic gait discovery for quadrupeds,” *Robotics and Automation Letters*, vol. 2, no. 3, pp. 1502–1509, July 2017.
- [9] I. Mordatch, E. Todorov, and Z. Popović, “Discovery of complex behaviors through contact-invariant optimization,” *ACM Transactions on Graphics (TOG)*, vol. 31, no. 4, p. 43, 2012.
- [10] M. Kalakrishnan, J. Buchli, P. Pastor, M. Mistry, and S. Schaal, “Fast, robust quadruped locomotion over challenging terrain,” in *ICRA*, May 2010, pp. 2665–2670.
- [11] C. D. Bellicoso, F. Jenelten, C. Gehring, and M. Hutter, “Dynamic locomotion through online nonlinear motion optimization for quadrupedal robots,” *IEEE Robotics and Automation Letters*, no. 99, 2018.
- [12] A. Hereid, E. A. Cousineau, C. M. Hubicki, and A. D. Ames, “3d dynamic walking with underactuated humanoid robots: A direct collocation framework for optimizing hybrid zero dynamics,” in *ICRA*, May 2016, pp. 1447–1454.
- [13] D. Pardo, M. Neunert, A. Winkler, R. Grandia, and J. Buchli, “Hybrid direct collocation and control in the constraint-consistent subspace for

- dynamic legged robot locomotion,” in *RSS*, 2017.
- [14] A. Werner, B. Henze, F. Loeffl, S. Leyendecker, and C. Ott, “Optimal and robust walking using intrinsic properties of a series-elastic robot,” in *2017 IEEE-RAS 17th International Conference on Humanoid Robotics (Humanoids)*, Nov 2017, pp. 143–150.
- [15] N. K. Gupta, “Frequency-shaped cost functionals-extension of linear-quadratic-gaussian design methods,” *Journal of Guidance, Control, and dynamics*, vol. 3, no. 6, pp. 529–535, 1980.
- [16] F. Farshidian, M. Neunert, A. W. Winkler, G. Rey, and J. Buchli, “An efficient optimal planning and control framework for quadrupedal locomotion,” in *ICRA*. IEEE, 2017, pp. 93–100.
- [17] F. Farshidian, E. Jelavic, A. Satapathy, M. Gifthaler, and J. Buchli, “Real-time motion planning of legged robots: A model predictive control approach,” in *2017 IEEE-RAS 17th International Conference on Humanoid Robotics (Humanoids)*, Nov 2017, pp. 577–584.
- [18] J.-H. Hours, M. N. Zeilinger, R. Gondhalekar, and C. N. Jones, “Constrained spectrum control,” *IEEE Transactions on Automatic Control*, vol. 60, no. 7, pp. 1969–1974, 2015.
- [19] J. Doyle and G. Stein, “Multivariable feedback design: Concepts for a classical/modern synthesis,” *IEEE transactions on Automatic Control*, vol. 26, no. 1, pp. 4–16, 1981.
- [20] F. Farshidian, E. Jelavic, A. W. Winkler, and J. Buchli, “Robust whole-body motion control of legged robots,” in *Intelligent Robots and Systems (IROS), 2017 IEEE/RSJ International Conference on*. IEEE, 2017, pp. 4589–4596.
- [21] B. Anderson and D. Mingori, “Use of frequency dependence in linear quadratic control problems to frequency-shape robustness,” *Journal of Guidance, Control, and Dynamics*, vol. 8, no. 3, pp. 397–401, 1985.
- [22] B. D. O. Anderson, J. A. Gibson, and H. R. Sirisena, “Phase lag and lead weighting in linear-quadratic control,” *Optimal Control Applications and Methods*, vol. 6, no. 3, pp. 249–263.
- [23] J. Albersmeyer and M. Diehl, “The lifted newton method and its application in optimization,” *SIAM Journal on Optimization*, vol. 20, no. 3, pp. 1655–1684, 2010.
- [24] C. D. Bellicoso, C. Gehring, J. Hwangbo, P. Fankhauser, and M. Hutter, “Perception-less terrain adaptation through whole body control and hierarchical optimization,” in *Humanoid Robots, 2016 IEEE-RAS 16th International Conference on*. IEEE, 2016, pp. 558–564.
- [25] Z. Gan, T. Wiestner, M. A. Weishaupt, N. M. Walder, and C. D. Remy, “Passive dynamics explain quadrupedal walking, trotting, and tötting,” *Journal of computational and nonlinear dynamics*, vol. 11, no. 2, p. 021008, 2016.
- [26] R. Smith *et al.*, “Open dynamics engine,” <http://www.ode.org>, 2005.